Supporting Information for Tunable Light Emission by Electrically Excited Plasmonic Antenna

Jin Qin[1, †], Yingjian Liu[1, †], Huiwen Luo[1], Zhongjun Jiang[1], Wenshan Cai[2,], and Liang Wang[1,*]*

[1]*Department of Optics and Optical Engineering, University of Science and Technology of China, Hefei City, Anhui Province 230026, China*

[2]*School of Electrical and Computer Engineering, Georgia Institute of Technology, Atlanta, Georgia 30332, United States*

†These authors contributed equally to the present work.

1. Plasmonic nanoantenna geometry

The plasmonic antenna has three main geometric parameters, comprising the bowtie angle, width and height, as indicated in Figure. S1a. SEM images of antennas with different parameters are shown below in Figure. S1b–g.

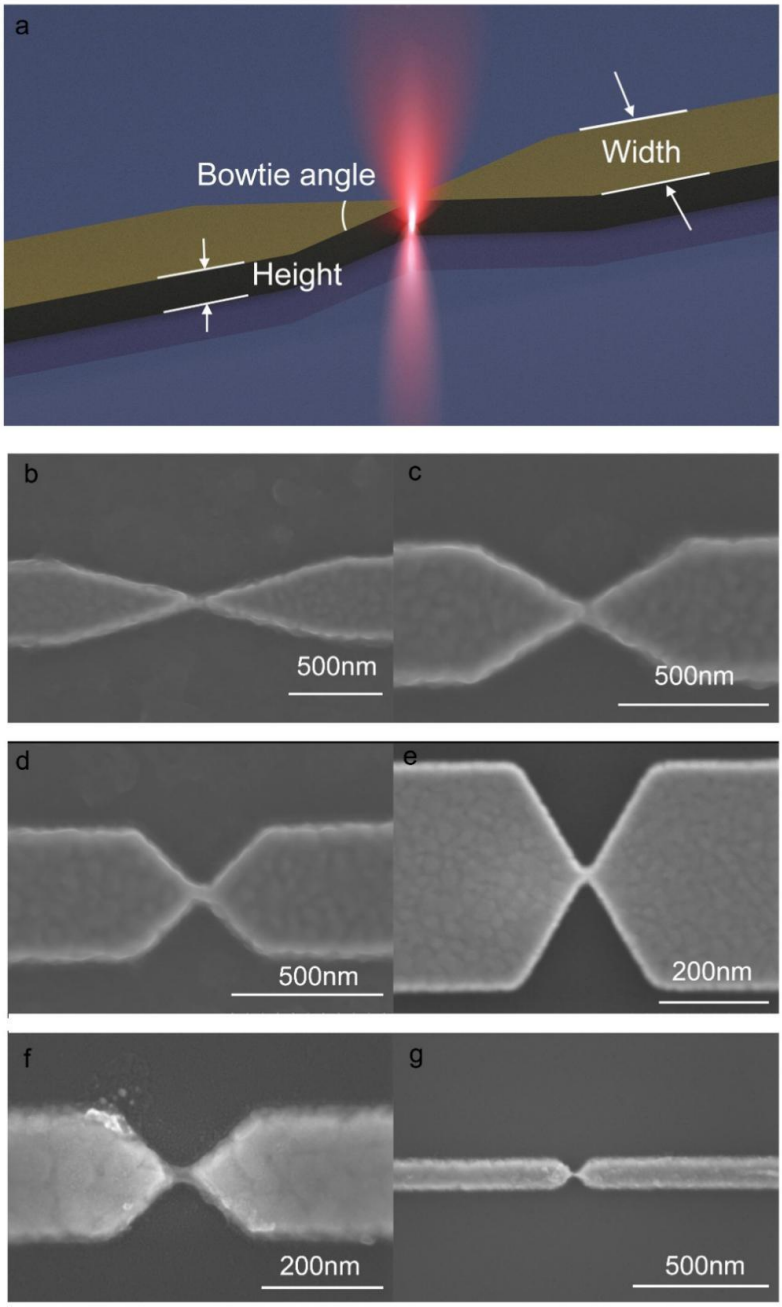

Figure. S1. Plasmonic nanoantenna geometry. (a) Sketch of the nanoantenna. (b–g)

SEM images of different nanoantennas. (b) Nanoantenna with width of 400 nm and bowtie angle of 30°. (c) Nanoantenna with width of 400 nm and bowtie angle of 60°. (d) Nanoantenna with width of 400 nm and bowtie angle of 90°. (e) Nanoantenna with width of 400 nm and bowtie angle of 120°. (f) Nanoantenna with width of 200 nm and bowtie angle of 90°. (g) Bowtie-type nanoantenna with width of 100 nm and bowtie angle of 90°.

2. Sample fabrication

The samples were fabricated via a two-step lift-off process. The procedure began with electron beam lithography (EBL, JEOL6300) performed on a glass coverslip (25 mm×25 mm×0.17 mm, Fisher 12-548C) that was coated with 150-nm-thick polymethyl methacrylate (PMMA). The exposure dose was accurately controlled to obtain a good connection for the antenna. Before a 50-nm-thick gold layer was deposited, a 5-nm-thick Ti layer was evaporated on the coverslip to act as an adhesion layer. The unpatterned area was removed via the lift-off process. The macroscopic contact pad was aligned and exposed via ultraviolet (UV) lithography after a 5-nm-thick Ti layer and a 150-nm-thick gold layer had been evaporated on it. Then, a second lift-off process was performed to produce the final structure. The detailed process flow is illustrated in Figure. S2.

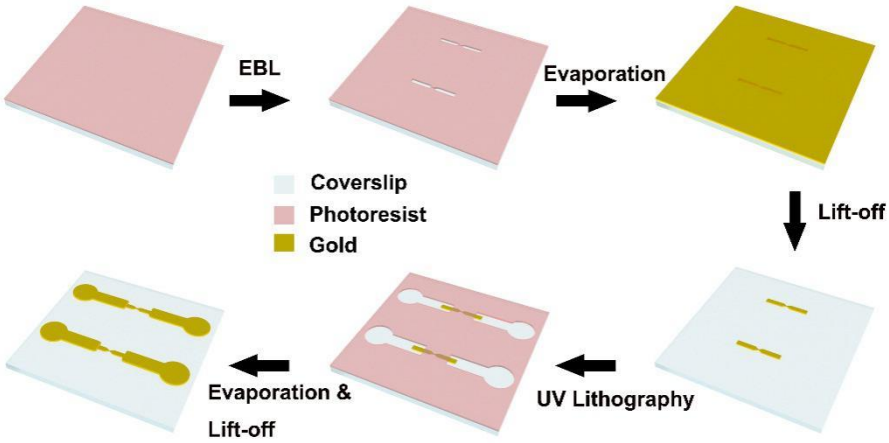

Figure. S2. Process flow chart.

3. Electromigration

Electromigration (EM) is a physical phenomenon that involves atomic motion and rearrangement under high-density current flow. It was previously known as a failure mode in microelectronic circuits. However, EM can also be used to generate a nanoscale separation that is typically less than 1 nm through implementation of a well-controlled EM procedure. Our electrical instruments for this procedure include two probe stations with triaxial cables and a single channel source meter (Keithley 2450). Voltages are applied on the macroscopic contact pads via a probe station with triaxial cables to shield the pads from excess noise. In addition, the sensing current is limited to within 10 mA as the voltage varies from 0 V to 4 V. The time evolution of the conductance with the

applied voltage is recorded to depict the connection status of the bowtie-type nanoantenna. Specifically, when the connection becomes a single-atom contact (as shown in Figure. S3), the conductance will reach the quantum conductance G_0. When the conductance drops below G_0, the required separation is formed. From Figure. 1(c), two conductance drops occur at 0.6 V and 1.1 V, which correspond to the states of single-atom contact and separation, respectively.

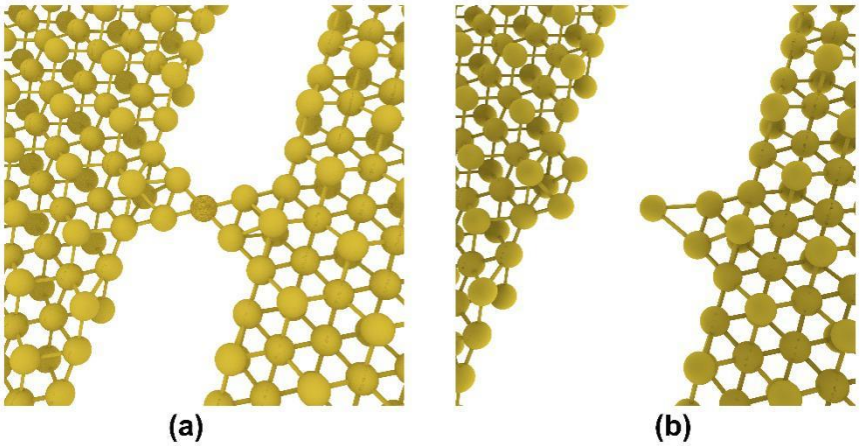

Figure. S3. Sketched geometries of the connection status. (a) Single-atom contact. (b) Nanogap formed by the EM process.

The EM process typically occurs at the weakest connection. Because of the intentional design of the plasmonic nanoantenna, the nanoscale separation will be accurately located at the tip centre. However, if the tiny connection at the tip centre is enlarged unexpectedly, a nanogap will form at random, as shown in the inset of Figure. S4. In this case, because the inelastic electron tunnelling (IET) is caused by the nanowire, the electroluminescence (EL) spectrum has only one peak with low output power (as shown in Figure. 4d).

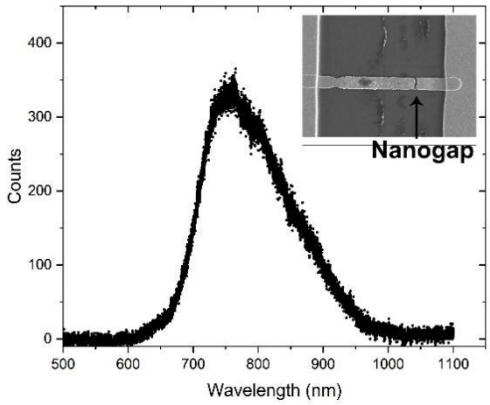

Figure. S4. EL spectrum of a nanowire. Inset: SEM image of bowtie-type nanoantenna after inappropriate EBL exposure dose. The tiny connection at the tip centre is close to that of the antenna. In addition, the EM process does not occur at the correct location.

4. Numerical simulations

To calculate the local density of optical states (LDOS) for both the nanoantenna and the nanowire, a model based on Green's function is established. The LDOS excited by a dipole is calculated using the dyadic Green's function, i.e.:

$$\nabla \times \nabla \times \overleftrightarrow{\mathbf{G}}(\mathbf{r},\mathbf{r}') - k^2 \overleftrightarrow{\mathbf{G}}(\mathbf{r},\mathbf{r}') = \overleftrightarrow{\mathbf{I}}\,\delta(\mathbf{r},\mathbf{r}')$$

Then, using Maxwell's equations, we obtain

$$\nabla \times \nabla \times \mathbf{E}(\mathbf{r}) - k^2 \mathbf{E}(\mathbf{r}) = i\omega\mu\mu_0 \mathbf{j}(\mathbf{r})$$

According to the two formulas shown above, the relationship between **E** and **G** can be written as

$$\mathbf{E}(\mathbf{r}) = i\omega\mu\mu_0 \int_V \overleftrightarrow{\mathbf{G}}(\mathbf{r},\mathbf{r}')\mathbf{j}(\mathbf{r}')dV'$$

where V is the space that surrounds the current density. When a dipole with moment $\boldsymbol{\mu}$ is used to replace the current density, the above formula can be rewritten as:

$$\mathbf{E}(\mathbf{r}) = \omega^2 \mu_0 \mu \overleftrightarrow{\mathbf{G}}(\mathbf{r}, \mathbf{r}')\boldsymbol{\mu}$$

where **r** is the field point that is generated by a dipole with moment **μ** located at the centre of the structure, and **r'** is the dipole position. As derived from the field intensity, ω is the frequency of the electromagnetic field radiated by the dipole. μ is the relative permeability and μ_0 is the permeability in free space. The Green's function at position **r** shows how the dipole at **r'** affects the electric field intensity at **r**. The tensor **G** can be solved as

$$\mathbf{G}_{i,j} = \frac{1}{\omega_0^{\ 2} \mu_0 \mu} \bullet \frac{\mathbf{E}_i}{\boldsymbol{\mu}_j}$$

Then, the LDOS can be expressed using Green's function:

$$\rho_\mu(\mathbf{r}_0, \omega_0) = \frac{6\omega_0}{\pi c^2}[\mathbf{n}_\mu \cdot \mathrm{Im}\{\overleftrightarrow{\mathbf{G}}(\mathrm{r}_0, \mathrm{r}_0; \omega_0)\} \cdot \mathbf{n}_\mu]$$

LDOS here refers to the electron-to-photon conversion efficiency, while the radiation efficiency indicates the percentage conversion of SPPs to free-space radiation. Both of these factors are spectrally dependent. The final electroluminescence spectrum can be expressed as:

$$p(\omega, V) \propto \Gamma_{e-p}(\omega, V)\eta_{antenna}(\omega)$$

where Γ_{e-p} represents the electron-to-photon conversion rate,

$$\Gamma_{e-p} \propto \frac{\rho_p}{\rho_0}(1 - \frac{\hbar\omega}{eV})$$

where ρ_p and ρ_0 are the LDOS and the DOS of a vacuum, and $\eta_{antenna}$ is the radiation efficiency of the antenna.

The LDOS is then calculated for both the plasmonic nanoantenna and the nanowire.

In the simulations, a tunnel gap of 0.6 nm was used at the centre of the bowtie antenna and the nanowire. From Figure. S5, we see that the LDOS of the bowtie antenna is much higher than that of the nanowire.

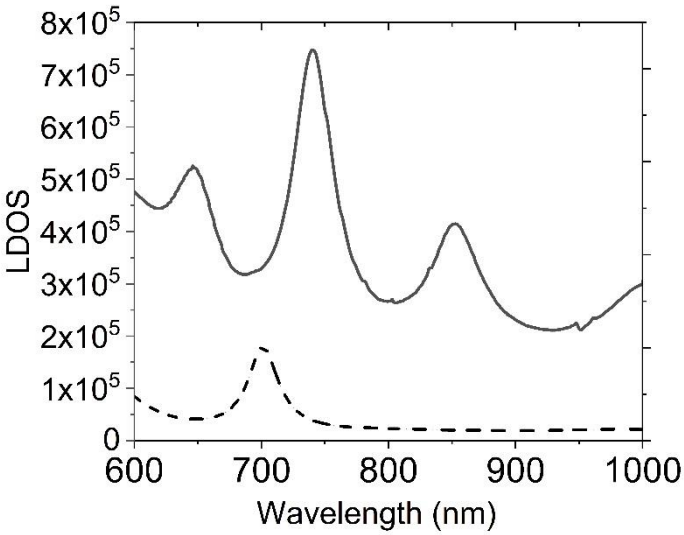

Figure. S5. LDOS of the plasmonic nanoantenna and the nanowire. The bowtie antenna has a width of 100 nm, height of 40 nm, and a bowtie angle of 60°. The nanowire width is 100 nm.

In the simulations, the LDOS is modified using the correction factor $(1\text{-}\hbar\omega / eV)$. A comparison of the experimental and theoretical spectra is shown in Figure. S6. When the bias voltage is less than 1.5 V, the emission spectrum only shows one peak because of the quantum limit. As the bias voltage gradually increases, LSP modes with higher energies emerge.

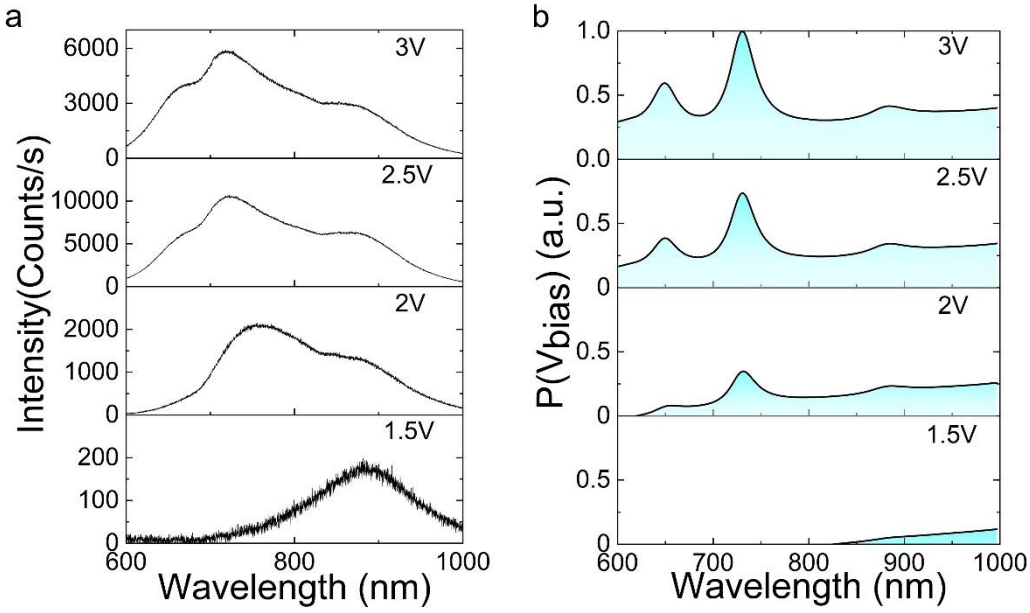

Figure. S6. Spectral evolution under different biases. (a) Spectra under different voltages ranging from 1.5 V to 3 V. (b) Simulated spectra produced by combining the correction factor and the LDOS.

Numerical simulation of the LDOS and radiation efficiency

Finite-difference time-domain (FDTD) method simulations were performed using Lumerical FDTD solutions software. Plasmonic antennas arranged along the *x*-direction are constructed with a gap of 0.6 nm. The dipole with the *x*-dipole vector is located in the gap in the antenna. A finer mesh grid of 0.2 nm×0.2 nm×0.2 nm per unit is generated near the gap. The substrate material is silicon dioxide, which has a refractive index of 1.5. The titanium adhesion layer could be ignored in the simulations. However, because of the interaction of the gold antenna with the dipole within the sub-nanometre gap, the nonlocal effects should not be neglected. The structure near the gap was quantized into 10 effective layers with different *d* parameters and the permittivity

was defined using the modified Drude model:

$$\varepsilon(d) = 1 - \frac{\omega_g^{\ 2}}{\omega(\omega + i\gamma_g(d))}$$

where d is the separation distance of the different pairs of layers, ω_g is a function with the Fermi energy of the metal and d was modified from the plasma frequency of the free electron gas to fit gold. The damping frequency γ_g is a function with a dependence on d.

$$\gamma_g(d) = \gamma^{gold} \exp(2qd)$$

Where $q = 1.12 \times 10^{10} m^{-1}$ according to the previous work. In addition to deduction from the Green's function, the LDOS can also be calculated by extracting the power from the simulation files. By placing a dipole p_x at the centre of the tunnel junction, the LDOS can be expressed as:

$$\rho_p = \rho_0 \times \frac{P_{tot}}{P_0}$$

where $\rho_0 = \omega^2 \pi^{-2} c^{-3}$, P_{tot} is the total dissipated power, and P_0 is the radiated power from a dipole in a homogeneous dielectric environment. The radiation efficiency is calculated from

$$\eta_{antenna} = P_{rad} / P_{tot}$$

where P_{rad} is the radiated power and P_{tot} is again the total dissipated power.

5. Optical setup

The optical system is built on the basis of back focal plane collection. This is very convenient in that it allows the probe station access to apply voltages to the electrodes. The optical system is illustrated in Figure. S7.

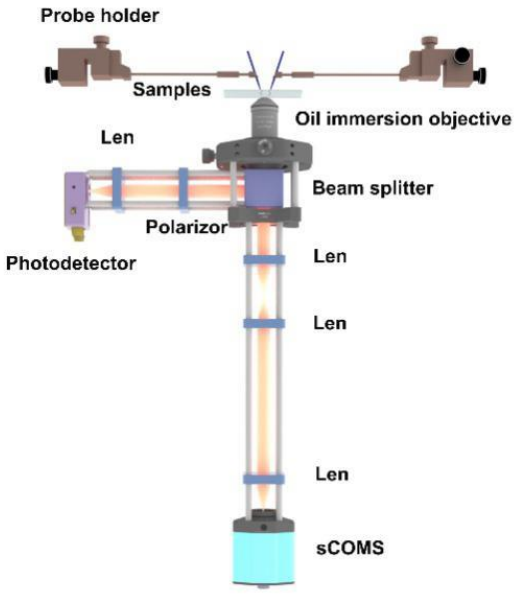

Figure. S7. Optical detection apparatus.

The electroluminescence is collected via an oil immersion objective (NA: 1.30; 100×, Olympus) The collected light is then separated by a 50/50 beam splitter. One beam is captured by a scientific camera (sCMOS, CS2100M-USB), while the other beam is collected to measure the electroluminescence power using a picowatt photodetector (PDF10A/M, Thorlabs) Both the Fourier plane and the image plane of the electroluminescence are recorded. Power variations with different polarizations are also recorded. The electroluminescence spectrum is measured using a spectrometer (Horiba, ISR550), which is equipped with a Synapse CCD detector.

6. Simmons fitting

To fit the *I-V* curve of the tunnel junction, a modified Simmons model with image potential is expressed below:

$$I = J_0\{\varphi_I \exp(-A\varphi_I^{\frac{1}{2}}) - (\varphi_I + eV)\exp[-A(\varphi_I + eV)^{\frac{1}{2}}]\}$$

where

$$J_0 = \frac{e}{2\pi h(\beta\delta s)^2}, \quad A = (4\pi\beta\delta s / h)\cdot\sqrt{2m},$$

h is Planck's constant and *m* is the mass of the electron. β is a potential correction factor. φ_I and *s* are both fitting parameters. The determination coefficient is calculated to be $R^2 = 0.9964$.

The Fowler-Nordheim characteristics were also fitted as shown in Figure. S8.

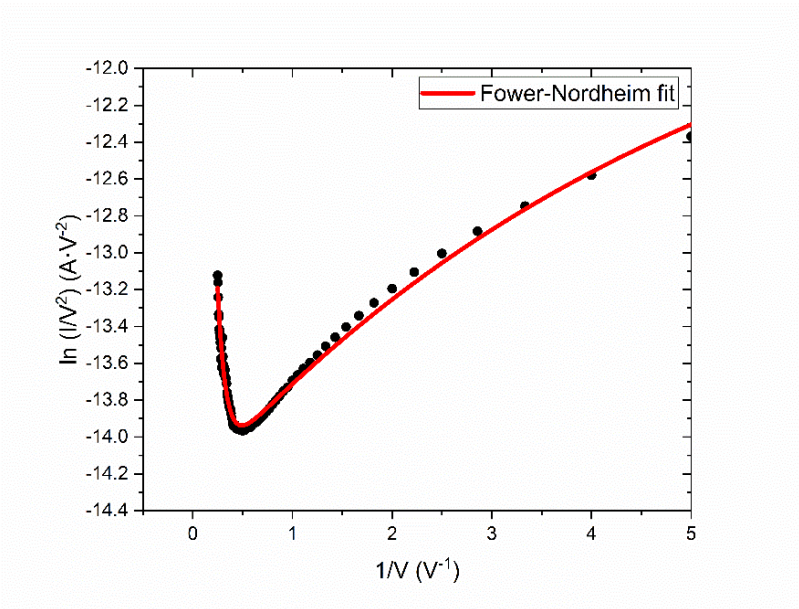

Figure. S8. Fowler-Nordheim characteristics of the tunnel junction.

7. Tunneling current compared with previous work

Tunneling current of different papers are compared in Table S1. a smaller gap generally gives a higher tunnel current under the same bias voltage.

References	Width of the tunnel gap	Tunnel current	Type of the tunnel junction	Output power	Measuring tool
7	1.3nm	~2nA(1.5V bias voltage)	Au-air-Au junction	/	EMCCD
9	2nm	~10nA	Au-Al_2O_3-Al junction	/	EMCCD
3	1.1nm	~10nA(1.5V bias voltage)	Au-air-Au junction	/	EMCCD
8	1.5nm	~25nA(2.5V bias voltage)	Ag-PVP-Ag junction	30pW	EMCCD
26	30nm	~100nA(15V bias voltage)	Au-air-Au junction	/	EMCCD
This work	0.6nm	~5μA(2.5V bias voltage)	Au-air-Au junction	1.4nW	CCD/sCMOS

Table S1 A comparison on light emission from nanogaps

8. Details of EQE measurement and calculation

We have measured about 30 samples to prove our EQE, the statistics results are shown as Figure. S9. Most of them have similar tunnel current (in the order of several micro Amperes) and the EQE is in the range of (5~20)$\times 10^{-5}$. The randomness of EQE may be caused by different geometric parameters of tunnel junction. And the roughness of sidewall will affect the propagation loss of the nanosources.

Preparation of the nanogaps by EM plays an important role in light emission. In our experiment, we also encountered some situations when the tunnel current is just a few nano amperes. And the emission light cannot be detected by our sCMOS.

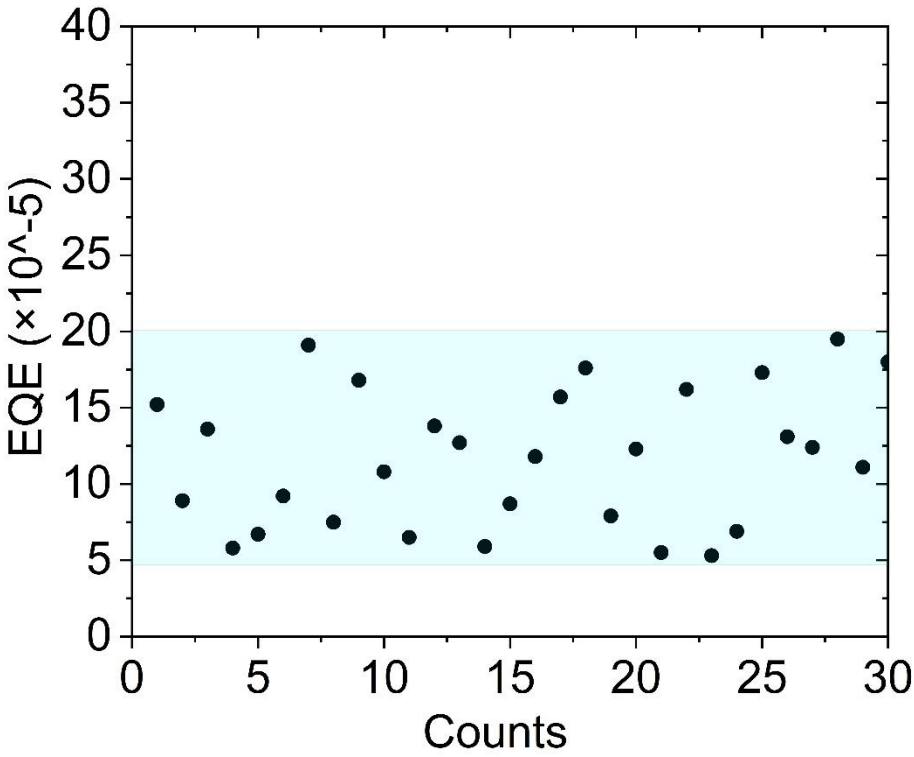

Figure. S9. The statistics EQE results of the nanosouces with 30 measures.

The quantum efficiency is the ratio of the counts of photons and the electrons. The counts of photons can be deduced from the output power. The counts of electrons is calculated as $\frac{W_{output}}{hv}$, where the energy of the electrons is decided by the bias voltages. The emission power of the device is detected by PDA. Light impinging on the detector is converted to the electrical signal with quantum efficiency. Thus the power of the light can be calculated from the spectrum.